Evaluation of porosity change during chemo-mechanical compaction in flooding experiments on Liège outcrop chalk

WENXIA WANG[1,2], MERETE V. MADLAND[1,2], UDO ZIMMERMANN[1,2]*, ANDERS NERMOEN[2,4], REIDAR I. KORSNES[1,2], SILVANA R. A. BERTOLINO[3] & TANIA HILDEBRAND-HABEL[2,4]

[1]*Department of Petroleum Technology, University of Stavanger, Norway*

[2]*The National IOR Centre of Norway, University of Stavanger, Ullandhaug, 4036 Stavanger, Norway*

[3]*FaMAF, Universidad Nacional de Córdoba, Medina Allende s/n, Ciudad Universitaria, Córdoba, Argentina*

[4]*IRIS AS, International Research Institute of Stavanger, Ullandhaug, 4036 Stavanger, Norway*

**Correspondence: udo.zimmermann@uis.no*

Abstract: The mechanical strength, porosity and permeability of chalk are affected by chemical and mineralogical changes induced by fluids that are chemically out of equilibrium with the host rock. Here, two high-porosity Upper Cretaceous chalk cores from Liège were tested at effective stresses beyond yield at 130°C during flooding with $MgCl_2$ and NaCl brines. Core L1 (flooded by $MgCl_2$ brine) deformed more than L2 (flooded with NaCl brine), with volumetric strains of 9.4% and 5.1%, respectively. The porosity losses estimated from strain measurements alone are 5.82% for L1 and 3.01% for L2. However, this approach does not account for dissolution and precipitation reactions. Porosity calculations that are based on strain measurements in combination with (i) the weight difference between saturated and dry cores and (ii) the solid density measurement before and after flooding show an average porosity reduction of 3.69% between the two methods for L1. This discrepancy was not observed for core L2 (with the NaCl brine). The rock and effluent chemistry show that Ca^{2+} dissolved and Mg^{2+} is retained within the core for the L1 experiment. Therefore, accurate porosity calculations in chalk cores that are flooded by non-equilibrium brines (e.g. $MgCl_2$) require both the volumetric strain and chemical alteration to be considered.

Chalk strength, which is associated with the elastic moduli, the onset of yield and the rates of deformation, has been the focus of several research communities since the 1980s, when the subsidence in the Ekofisk field (Norwegian North Sea) was discovered (Wiborg & Jewhurst 1986). Seawater injection was initiated in 1987 to improve the oil production and to stop or reduce subsidence. Oil production improved significantly, but reservoir compaction in the water-saturated regions continued, in contrast to the regions with no water breakthrough. This observation indicates the existence of a water weakening effect on the chalk's mechanical properties. Numerous studies have since been initiated to improve the understanding of: (i) the relation between the pore fluid composition and mechanical properties (Newman 1983; Madland 2005; Korsnes *et al.* 2006*a*, *b*); (ii) the effect of mechanical strength as temperature decreases during injection (Korsnes *et al.* 2008; Madland *et al.* 2008); and (iii) the relation between the changed brine chemistry and deformation rates under constant stress conditions (e.g. Hellmann *et al.* 2002; Korsnes 2007; Madland *et al.* 2011; Nermoen *et al.* 2015).

During the continuous injection of brines such as synthetic seawater (SSW) that are not in chemical equilibrium with the host rock, equilibrium calculations at the pressures and temperatures relevant to some reservoirs indicate that the brines are supersaturated in terms of Mg^{2+}, leading to the precipitation of new mineral phases (Hiorth *et al.* 2008). Consequently, the fluids become undersaturated in other elements such that additional secondary dissolution is triggered (Madland *et al.* 2011). In contrast, chalk flooding experiments with simpler brines, such as $MgCl_2$, which are not in equilibrium with the host

From: Armitage, P. J., Butcher, A. R., Churchill, J. M., Csoma, A. E., Hollis, C., Lander, R. H., Omma, J. E. & Worden, R. H. (eds) *Reservoir Quality of Clastic and Carbonate Rocks: Analysis, Modelling and Prediction*. Geological Society, London, Special Publications, **435**, http://doi.org/10.1144/SP435.10

rock, show that the dissolution of minerals may lead to the precipitation of Mg-bearing carbonate minerals (Madland *et al.* 2013).

The chalk reservoir at Ekofisk field (North Sea) is currently undergoing compaction during seawater injection, despite the reduction in effective stress. An increase in pore pressure will usually reduce or even stop compaction when no chemical interaction between the rock and brine is taking place. Reservoir compaction by pore volume reduction is an important driving mechanism that forces pore fluids towards the production wells. At the same time, the reduction in pore volume changes the flow properties (i.e. by reducing the permeability) of the reservoir. To support qualified reservoir management decisions and EOR implementation it is therefore important to have accurate estimates of the pore space evolution during fluid injection.

The objective of this article is to show that the non-equilibrium nature of the rock–fluid interface induces mineralogical changes and to demonstrate how those mineralogical changes affect the mechanical properties of the rock. These results lead to a more accurate way of estimating porosity compared with using bulk volumetric strain alone. This approach is necessary because significant changes in the mass and density, and hence, the solid volume, occur during the injection of fluids that are chemically out of equilibrium with the host chalk rocks. This effect also may also be relevant for other reservoir rock types where chemo-mechanical interactions occur.

Methods and experimental procedures

Core material and flooding fluids

Large sample blocks were taken from the quarry close to Hallembaye (Cimenterie Belge Reunié (CBR) Lixhe quarry; Slimani 2001) which is situated in the Liège region (Belgium) at 50°44′ 51.16″N and 05°38′52.17″E. The petrology, mineralogical and rheological characteristics of the chalk have been studied in detail (Felder 1975; Molenaar & Zijlstra 1997; Slimani 2001; Strand *et al.* 2007; Hjuler & Fabricius 2009). The porosity varies between 40% and 45% and the chalk is composed of *c.* 97% carbonate minerals.

In this study, 0.219 M $MgCl_2$ and 0.657 M NaCl were used as the injection fluids (Table 1).

Experimental preparation and procedure

Two samples were drilled from a large chalk block and machined into cylindrical shapes with initial diameters of 37.05 and 38.15 mm and lengths of 68.88 and 72.65 mm for tests L1 and L2, respectively. Because both cores have a length to diameter ratio that is close to two their strengths should be insensitive to differences in their diameters (Fjær *et al.* 2008). After preparation, both cores were dried for 12 h in a heating chamber at 100°C to remove more than 99% of the water in the core before the dry mass was determined. The calcite crystals are unaffected by the drying conditions. Then the cores were evacuated by vacuum before being saturated with distilled water and weighed to obtain the saturated mass. The difference between the saturated and dry masses is attributed to the mass of the pore water, which is then used to estimate the pore volume fraction (i.e. porosity). The same experimental procedure was used on both cores. The saturated cores were mounted into two identical triaxial cells (see Fig. 1 for a description of the set-up). The cells were equipped with a heating jacket and a regulating system (Omron E5CN) with precise proportional integral derivative (PID) temperature control (± 0.1°C). Three Gilson (model 307 HPLC) pressure pumps were connected to each triaxial cell enabling the independent control of the piston pressure, the confining pressure (radial stress) and the injected flow rate (i.e. pumps 1–3 in Fig. 1). The confining pressure balances the piston such that the axial stress has to be calculated from the confining pressure plus the piston pressure, (see equation 1 in Nermoen *et al.* 2015). A back-pressure regulator was placed downstream of the core to control the pore pressure and allow for continuous sampling of the effluent fluids. To isolate the cores from the confining oil, a heat shrinkage sleeve (1–1/2″ FEP with a diameter of 33–43 mm and a wall thickness of 0.5 mm) was installed between the core and

Table 1. Injected brine composition for tests L1 and L2, flow rate and test duration

Test	Flow rate (ml min^{-1})	Test duration (days)	Cl^- (mol l^{-1})	Mg^{2+} (mol l^{-1})	Na^+ (mol l^{-1})	Ion strength (mol l^{-1})	TDS (g l^{-1})
L1	0.022	65	0.438	0.219	0	0.657	20.84
L2	0.025	90	0.657	0	0.657	0.657	38.40

TDS, total dissolved solids.

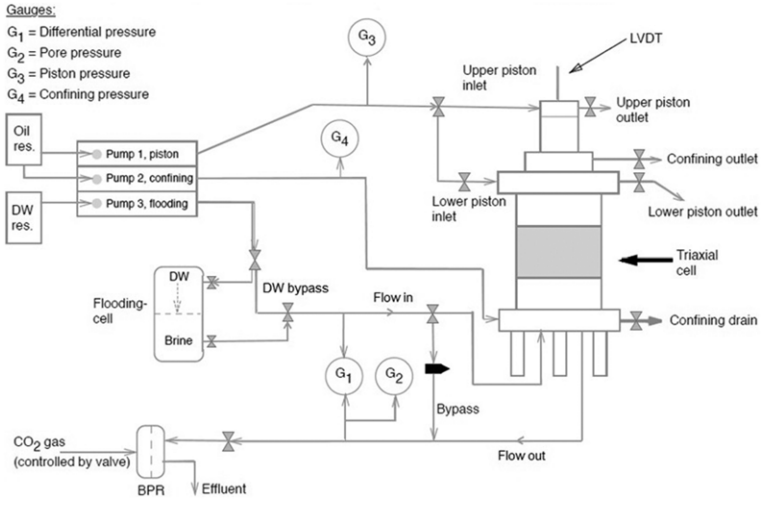

Fig. 1. The triaxial cell used in the flooding tests. Three pumps (the piston, confining and flooding pumps) were connected to the cell. The flooding cell contained DW (upper chamber) and $MgCl_2$/NaCl (lower chamber). During the flooding period the cell was refilled as soon as the fluid ran out. This whole set-up was connected to the computer and complete data, including the confining, pore and piston pressures, flooding rate and time, were logged automatically.

the confining oil. After core mounting, the confining pressure was increased to 0.5 MPa. Thereafter the experiments were conducted according to the following stages:

(1) The samples were flooded with three pore volumes (PVs) of distilled water (DW) overnight at ambient temperature to remove any salt precipitates that could affect the flooding test. This flooding procedure does not significantly alter the geochemical measurements of the non-salt minerals in the core.

(2) Flooding was then switched to an $MgCl_2$ brine for L1 and an NaCl brine for L2, by attaching the piston cell into the flow loop (see Fig. 1). The ion compositions of the injected brines are shown in Table 1. Throughout the rest of the test, the flow rate was set to one initial PV per day, which corresponds to 0.022 and 0.025 ml min^{-1} for L1 and L2, respectively (Table 1).

(3) The confining pressure and pore pressure were increased to 1.2 and 0.7 MPa, respectively, before the temperature was raised to 130°C. The pore pressure and temperature were subsequently kept constant throughout the test.

(4) The confining pressure was increased from 1.2 MPa by injecting hydraulic oil into the confining chamber at a constant flow rate using pump 2. During pressurization the piston pressure was set to 0.5 MPa to slightly exceed friction of the piston (0.3–0.4 MPa). This increased the axial stress to a value of 0.1–0.2 MPa above the radial stress. Because the additional axial stress is small compared with the radial stress, the stress condition can be considered near-hydrostatic. The axial strain was measured by an external axial linear variable displacement transducer (LVDT) placed on top of the piston to monitor the sample length with time. The stress–strain behaviour was monitored as the confining pressure was increased (see Fig. 2). When the rock began to deform plastically (Fig. 3), i.e. when the stress–strain behaviour became non-linear, the stress at the onset of yield was noted (7.5 and 8.5 MPa for L1 and L2, respectively). The targets for the confining pressure were selected to be 2 MPa above the yield stress, i.e. 9.5 and 10.5 MPa for cores L1 and L2.

(5) The axial deformation at constant temperature, stress and pressure conditions (termed creep) was monitored for 65 and 90 days during continuous flooding with $MgCl_2$ and NaCl brines for tests L1 and L2, respectively. The creep magnitude through time is shown in Figure 3. The pore pressure and confining pressure varied within 0.1 MPa such that the effective stresses were stable throughout the test period.

The pore pressure, hydraulic pressure difference, confining pressure, piston pressure, sample length (axial strain) and flooding time were logged

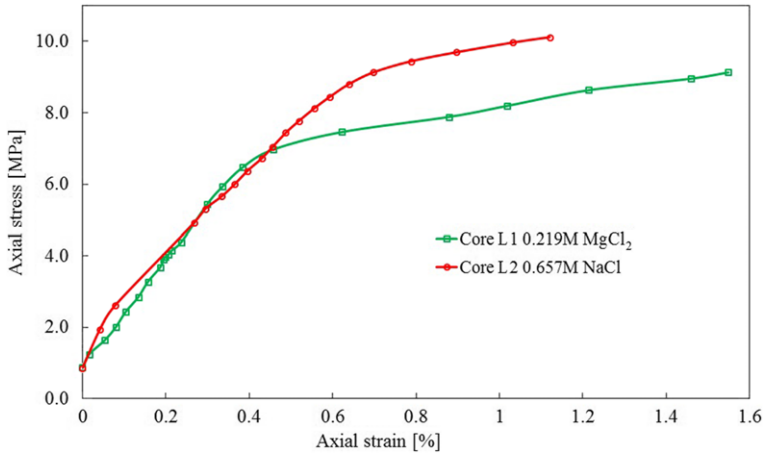

Fig. 2. Axial stress v. axial strain for the L1 and L2 cores flooded with $MgCl_2$ and NaCl, respectively, at 130°C. Note that L2 has higher yield point (8.5 MPa) than the core L1 (7.5 MPa).

continuously via a LabView programme. Before dismantling the core, the sample was cleaned by injecting three PVs of distilled water to avoid the precipitation of salts from the $MgCl_2$ and NaCl brines during drying. The saturated weight was measured immediately after the cell was dismantled. The core was then placed in the drying cabinet at 100°C and weighed several times until the mass stayed constant. Both experiments have been performed in the same way so the brine dependent behaviour can be identified. The basic core properties before and after flooding are presented in Table 2. Then the cores were cut into seven slices using a Struers Discotom-5 cutting machine. The slices were labelled FL1-1 to FL1-7 for flooded L1 and FL2-1 to FL2-7 for flooded L2 along the core axis from the inlet to the outlet (see Fig. 4 for the sectioning scheme). The slices were used for geochemical analyses of the rock to identify the mineralogical changes along the core.

Ion chromatography

During the experiment, the effluents of the samples were collected for chemical comparison between the produced and injected water. The ionic

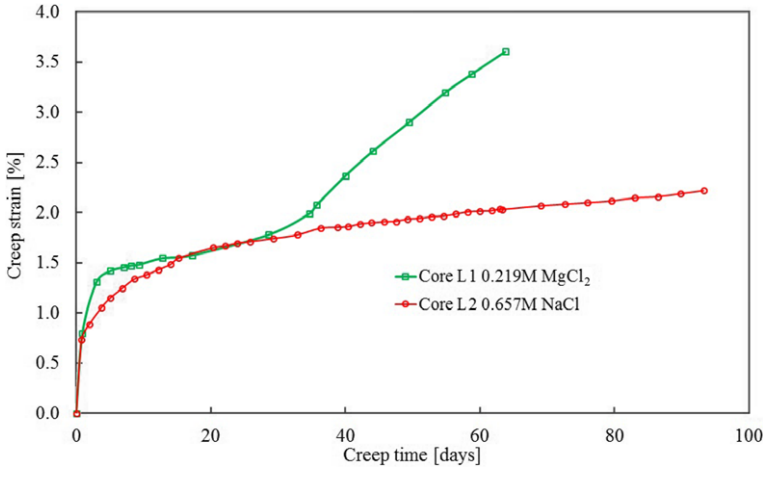

Fig. 3. Axial creep strain v. creep time for L1 and L2 under different creep stress at 130°C. The different creep stresses for L1 and L2 are 9.5 and 10.5 MPa respectively. Note that the L1 test accumulates more creep strain over 65 days than the L2 test, which was flooded for 90 days.

Table 2. *Basic core measurements before and after the tests performed at 130°C for L1 and L2, respectively*

Test	Initial core values										
	Length (mm)	Diameter (mm)	Dry mass (g)	Saturated mass (g)	Bulk volume (cm^3)	Solid volume (saturation) (cm^3)	Pore volume (saturation) (cm^3)	Porosity (saturation) (%)	Density (pycnometry) ($g\ cm^{-3}$)	Mineral density (saturation) ($g\ cm^{-3}$)	Solid volume (pycnometry) (cm^3)
L1 ($MgCl_2$ at 9.5 Mpa)	68.88	37.05	112.38	144.65	74.26	41.99	32.27	43.45	2.68	2.68	41.93
L2 (NaCl at 10.5 Mpa)	72.65	38.15	126.05	162.12	83.05	46.98	36.07	43.43	2.69	2.68	46.86

Test (three sets of FL1)	Flooded core material after the test										
	Vol. strain (%)	Dry mass (g)	Saturated mass (g)	Bulk volume (truncated wedge) (cm^3)	Density (pycnometry) ($g\ cm^{-3}$)	Solid volume (saturation) (cm^3)	Pore volume (saturation) (cm^3)	Solid volume (pycnometry) (cm^3)	Porosity (method 1) (%)	Porosity (method 2) (%)	Porosity (method 3) (%)
FL1	9.4	110.28	137.38	67.27	2.70	40.17	27.10	40.84	37.63	40.29	39.28
FL2	5.1	125.51	157.85	78.77	2.69	46.43	32.34	46.66	40.42	41.06	40.77

Comparison of the dry and DW-saturated weights with the solid volume, pore volume and porosity (ϕ) estimates based on both saturation and the pycnometer results from Table 3. In addition, volumetric strains and porosities are estimated using the methods 1–3 as explained in the 'Porosity calculation' section. Indices s1 to s7 relate to the position along the axis of the sample from inlet to outlet (see Fig. 4). 'Test' indicates three sets of tests for FL 1.

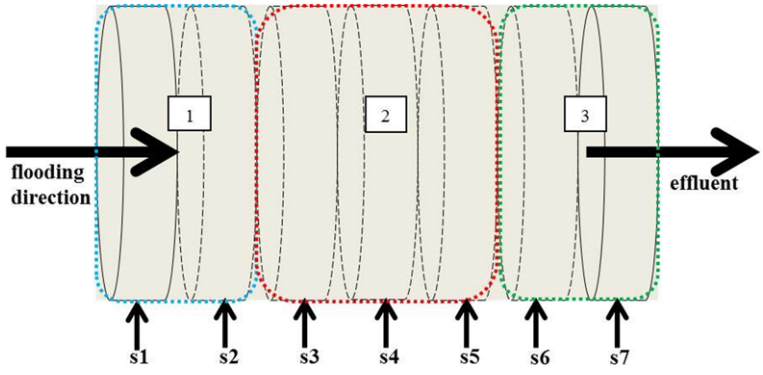

Fig. 4. Schematic of the sectioning of the core after the experiment. The subsamples were analysed using different methods. The inlet is at s1 and the outlet at s7. The samples were grouped as indicated (1–3) for pycnometry measurements.

concentrations were analysed with a Dionex ICS-3000 ion-exchange chromatograph. The analyses were performed with an ICS 3000 CD Conductivity Detector. IonPac AS16 and IonPac CS12A were used as the anion and cation exchange columns, respectively. The sampled effluents were diluted (Gilson, GX-271) to stay in the linear region of the calibration curve and the ionic concentrations were calculated on the basis of an external standard (SMOW; standard mean ocean water). The following ions have been quantified and plotted through time in Figure 5: Mg^{2+}, Na^{+}, Cl^{-} and Ca^{2+}.

Pycnometry

The solid volume was measured with an AccuPyc II 1340 gas pycnometer, which measures the amount of displaced helium gas within a porous rock sample. The dry sample was placed into the volume chamber and helium gas molecules rapidly filled the pores. A chamber of 35 cm^3 was selected to provide the best fit with the samples. Estimates of the average mineral densities were obtained based on the solid volume and dry mass (see Table 3). The pycnometry measurements represent a complementary way of estimating the porosity, in addition to the porosity estimate from the difference between the dry and DW-saturated cores.

Field emission gun scanning electron microscopy (FEG-SEM)

The fresh surfaces from each slice (Fig. 4) were analysed using a Zeiss Supra 35VP field emission SEM in high vacuum mode with an accelerating voltage of 12 kV, an aperture size of 30 μm and a working distance of 10–12 mm. EDAX Genesis energy-dispersive X-ray spectroscopy (EDS) was used to determine the mineralogical and elemental compositions of the chalk samples. Because the core dominantly consisted of calcite, the EDS system was calibrated using an Iceland spar calcite crystal before the samples were analysed.

X-Ray diffraction

X-Ray diffraction patterns were obtained from bulk samples of the different slices (in Fig. 4) in random mounts using a Bruker D5005 diffractometer, Cu–Kα radiation, 0.02° per step at 1 s per step. The measurements were repeated in certain samples to evaluate the reproducibility of the results; particularly for cases involving newly formed trace minerals. The available amount for measurements was around 1 g. The XRD analyses were performed at the Institute of Earth Sciences Jaume Almera (ICTJA, Barcelona, Spain).

Whole-rock geochemistry

Representative sample material from each slice (see Fig. 4) was carefully separated from the core and milled to a very fine mesh in a clean agate mill. Geochemical data were obtained by inductively coupled plasma mass spectrometry (ICP-MS) analysis at Acme laboratory (Vancouver, Canada). Details of the analytical method and processing technique can be found at http://acmelab.com but are summarized here. The samples were first ground in an agate mill. The milled sample was then mixed with an $LiBO_2/Li_2B_4O_7$ flux in crucibles and fused in a furnace. The cooled bead was dissolved in ACS grade nitric acid and analysed by ICP-MS. Loss on ignition (LOI) was determined by igniting a sample split then measuring the weight loss. A 1 g sample was weighed into a tarred crucible and ignited to 1000°C for 1 h before being cooled and weighed again. The loss in weight is the LOI of the sample.

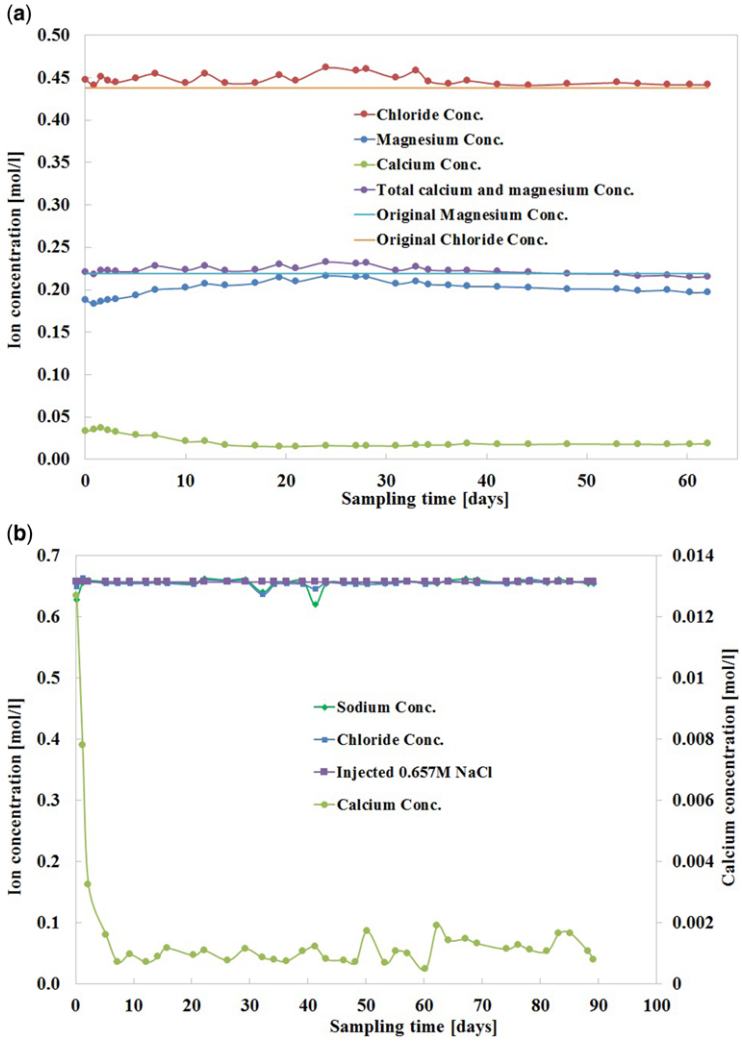

Fig. 5 (**a**) Mg^{2+}, Ca^{2+} and Cl^{-} concentrations in the sampled effluent from core L1 flooded with a 0.219 M $MgCl_2$ brine. (**b**) Na^{+}, Ca^{2+} and Cl^{-} concentrations in the sampled effluent from core L2 flooded with 0.657 M NaCl. The test temperature was set to 130°C. Sampling started after the hydrostatic loading was completed.

Table 3. *Densities obtained from pycnometer measurements of flooded core samples*

Pycnometry results		
Test	Slices	Density (g cm^{-3})
FL1	s1 + s2	2.71
	s3 + s4 + s5	2.70
	s6 + s7	2.70
FL2	s1 + s2	2.69
	s3 + s4 + s5	2.69
	s6 + s7	2.69

Total carbon and sulphur were determined by the Leco method. Here, an induction flux was added to the prepared sample then ignited in an induction furnace. A carrier gas sweeps up the released carbon to be measured by adsorption in an infrared spectrometric cell. The results are the total concentrations attributed to the presence of carbon and sulphur in all of the components. An additional 14 elements were measured after dilution in aqua regia. The prepared sample was digested with a modified aqua regia solution with equal parts concentrated HCl, HNO_3 and deionized water for one hour in a heating block or hot water bath. The sample volume was

Table 4A. *Data for the FL1 and FL2 cores and untested end pieces of the L1 and L2 cores from Liège: (A) Geochemical isotope concentrations. Orig., unflooded chalk sample; avg., average; A, unflooded sample adjacent to the inlet (s1 in Fig. 4); B, unflooded sample adjacent to the outlet (s7 in Fig. 4)*

	SiO_2 %	Al_2O_3 %	Fe_2O_3 %	MgO %	CaO %	Na_2O %	K_2O %	TiO_2 %	P_2O_5 %	MnO %	LOI %	Sum %
Orig. L1 – A	2.21	0.38	0.19	0.29	53.98	0.05	0.1	0.02	0.07	0.02	42.6	99.86
Orig. L1 – B	2.15	0.37	0.18	0.27	54.1	0.05	0.09	0.02	0.07	0.02	42.6	99.87
Orig. L1 (avg.)	**2.18**	**0.38**	**0.19**	**0.28**	**54.04**	**0.05**	**0.10**	**0.02**	**0.07**	**0.02**	**42.6**	**99.87**
FL1 (avg.)	**2.00**	**0.37**	**0.13**	**1.85**	**52.32**	**0.04**	**0.05**	**0.02**	**0.12**	**0.02**	**42.8**	**99.84**
Orig. L2 – A	1.92	0.32	0.24	0.27	54.21	0.04	0.07	0.02	0.14	0.02	42.6	99.85
Orig. L2 – B	1.89	0.32	0.20	0.27	54.14	0.04	0.07	0.02	0.13	0.02	42.8	99.85
Orig. L2 (avg.)	**1.91**	**0.32**	**0.22**	**0.27**	**54.18**	**0.04**	**0.07**	**0.02**	**0.14**	**0.02**	**42.7**	**99.85**
FL2 (avg.)	**1.85**	**0.34**	**0.13**	**0.28**	**54.62**	**0.06**	**0.05**	**0.02**	**0.10**	**0.02**	**42.3**	**99.86**
Slice 1 to 7 of the $MgCl_2$ – flooded core (Test ID: L1)												
FL1-1	1.70	0.33	0.12	1.72	52.84	0.03	0.04	0.02	0.10	0.03	42.9	99.83
FL1-2	2.00	0.39	0.13	2.34	51.51	0.03	0.05	0.02	0.11	0.02	43.2	99.83
FL1-3	2.09	0.39	0.15	3.21	50.76	0.04	0.06	0.02	0.18	0.03	42.8	99.82
FL1-4	2.09	0.40	0.12	2.07	51.94	0.04	0.06	0.02	0.16	0.02	42.8	99.84
FL1-5	2.06	0.37	0.16	1.38	52.60	0.04	0.06	0.02	0.12	0.02	42.9	99.85
FL1-6	2.09	0.37	0.13	1.16	53.24	0.04	0.06	0.02	0.08	0.02	42.5	99.85
FL1-7	1.95	0.35	0.12	1.04	53.37	0.04	0.05	0.02	0.11	0.02	42.7	99.85
Slice 1 to 7 of the NaCl – flooded core (Test ID: L2)												
FL2-1	1.44	0.27	0.10	0.30	54.41	0.04	0.04	0.02	0.05	0.02	43.1	99.85
FL2-2	1.80	0.35	0.15	0.26	55.46	0.04	0.05	0.02	0.09	0.02	41.6	99.85
FL2-3	1.76	0.33	0.18	0.27	55.68	0.05	0.05	0.02	0.07	0.02	41.4	99.85
FL2-4	1.96	0.35	0.15	0.28	54.72	0.05	0.06	0.02	0.10	0.02	42.0	99.86
FL2-5	1.97	0.37	0.10	0.29	54.13	0.06	0.06	0.02	0.13	0.02	42.6	99.87
FL2-6	1.97	0.36	0.11	0.29	54.16	0.07	0.06	0.02	0.13	0.02	42.6	99.87
FL2-7	2.05	0.38	0.12	0.28	53.77	0.08	0.06	0.02	0.11	0.02	42.9	99.87

increased with dilute HCl solutions and splits of 0.5 g were analysed. All of the measured concentrations fall within the standard range (see Table 4), and accuracy and precision are between 2% and 3%.

Constitutive relations and porosity calculations

At any time the bulk volume of a porous material (V_b) is given by the volume of the pores (V_p) plus the volume of the solids (V_s),

$$V_b = V_s + V_p \tag{1}$$

Porosity (ϕ, expressed as a percentage) is calculated from the ratio

$$\phi = \frac{V_p}{V_b} \tag{2}$$

The initial porosity (ϕ_0) is calculated by the difference between the saturated and dry weights ($M_{sat,0}$ and $M_{dry,0}$) divided by the density of distilled water (ρ_{DW}) multiplied by the initial bulk volume ($V_{b,0}$),

$$\phi_0 = \frac{M_{sat,0} - M_{dry,0}}{\rho_{DW} V_{b,0}} \tag{3}$$

After the experiment was finished and dismantled, the diameter (D_i) was measured at intervals (L_i) along the core to provide accurate estimates of the total bulk volume from the sum of the truncated wedges $i = 1, 2, \ldots, 7$ along the core,

$$V_{b,end} = \sum_i \frac{L_i \pi}{3}\left(\left(\frac{D_i}{2}\right)^2 + \left(\frac{D_i}{2}\right)\left(\frac{D_{i+1}}{2}\right) + \left(\frac{D_{i+1}}{2}\right)^2\right) \tag{4}$$

This procedure was used because the volumetric deformation was not uniform along the sample, i.e. radial deformation was greater near the centre of the core than the ends. The overall change in the bulk volume before and after testing was used to estimate the total volumetric strain ε_{vol}, expressed as a percentage according to

$$\varepsilon_{vol} = \frac{V_{b,0} - V_{b,end}}{V_{b,0}} \tag{5}$$

It is standard procedure in triaxial experiments to define the positive strain when the volume or length of the core plug is reduced. Given a porous material, as defined in equation (1), any change in

Table 4B. *Data for the FL1 and FL2 cores and untested end pieces of the L1 and L2 cores from Liège: (B) isotope geochemistry and selected trace element whole-rock geochemistry. Orig., unflooded chalk sample; avg., average; A, unflooded sample adjacent to the inlet (s1 in Fig. 4); B, unflooded sample adjacent to the outlet (s7 in Fig. 4)*

	Ba (ppm)	Rb (ppm)	Sr (ppm)	Zr (ppm)	Y (ppm)	ΣREE (ppm)	Total carbon	$\delta^{13}C_{SMOW}$ (‰)	$\delta^{18}O_{SMOW}$ (‰)	Temperature estimate (‰)
Orig. L1 – A	30.0	2.2	1008	5.3	7.4	21.8	11.9	1.495	−1.985	20.2
Orig. L1 – B	32.0	2.2	982	5.0	7.2	22.5	11.9	1.609	−1.670	18.8
Orig. L1 (avg.)	**31.0**	**2.2**	**995**	**5.2**	**7.3**	**22.1**	**11.9**	**1.552**	**– 1.828**	**19.5**
FL1 (avg.)	**12.1**	**2.7**	**961**	**9.5**	**8.1**	**25.6**	**12.4**	**1.592**	**– 2.049**	**20.5**
Orig. L2 – A	31.0	3.6	908	7.5	9.0	26.3	11.7	1.599	−1.911	19.9
Orig. L2 – B	35.0	3.6	912	8.8	8.2	23.9	12.0	1.803	−1.607	18.6
Orig. L2 (avg.)	**33.0**	**3.6**	**910**	**8.2**	**8.6**	**25.1**	**11.8**	**1.701**	**– 1.759**	**19.2**
FL2 (avg.)	**17.9**	**2.3**	**1007**	**7.7**	**7.5**	**24.1**	**12.6**	**1.652**	**– 1.887**	**19.8**
Slices 1–7 of the $MgCl_2$ – flooded core (Test L1)										
FL1-1	14.0	2.5	1007	7.2	7.1	23.1	11.9	1.549	−2.028	20.4
								1.591	−1.955	20.1
FL1-2	13.0	2.6	958	7.5	8.2	24.1	12.1	1.638	−1.991	20.2
								1.651	−2.017	20.3
FL1-3	12.0	2.7	891	8.9	9.2	26.8	12.5	1.498	−2.469	22.4
								1.542	−2.322	21.7
FL1-4	10.0	3.1	922	10.0	8.9	28.7	12.4	1.432	−2.312	21.7
								1.571	−2.115	20.8
FL1-5	12.0	2.9	963	11.5	8.3	25.3	12.7	1.613	−1.961	20.1
								1.674	−1.930	20.0
FL1-6	11.0	2.7	1008	11.0	7.0	25.7	12.6	1.697	−1.732	19.1
								1.630	−1.907	19.9
FL1-7	13.0	2.6	978	10.4	8.2	25.3	12.4	1.592	−1.995	20.2
								1.605	−1.947	20.0
Slices 1–7 of the NaCl – flooded core (Test L2)										
FL2-1	13.0	1.8	1043	8.1	7.1	23.4	12.5	1.686	−1.863	19.7
								1.627	−1.913	19.9
FL2-2	16.0	2.1	1039	5.7	7.4	22.5	12.7	1.661	−1.909	19.9
								1.647	−1.885	19.8
FL2-3	15.0	1.9	1034	5.6	7.0	21.9	12.7	1.663	−1.810	19.4
								1.662	−1.847	19.6
FL2-4	24.0	2.3	1020	7.8	8.2	24.7	12.8	1.614	−1.903	19.8
								1.625	−1.980	20.2
FL2-5	18.0	2.7	947	9.3	7.0	26.7	12.5	1.722	−1.852	19.6
								1.627	−1.903	19.8
FL2-6	19.0	2.5	968	8.6	8.2	23.3	12.6	1.637	−1.880	19.7
								1.672	−1.846	19.6
FL2-7	20.0	2.8	997	9.0	7.8	26.5	12.8	1.642	−1.898	19.8
								1.641	−1.933	20.0

*Palaeo- and flooding temperatures have been calculated after Anderson & Arthur (1983) with salinity values taken from Wright (1987). Highlighted in grey are the significant chemical changes discussed in the text. **Bold**, average values for the different samples.

the bulk volume (ΔV_b) is given by the change in the solid volume (ΔV_s) plus the change in the pore volume (ΔV_p),

$$\Delta V_b = \Delta V_s + \Delta V_p \quad (6)$$

If all of the deformation is accommodated by the reduction in pore volume and the solid volume remains constant ($\Delta V_s = 0$) (either there is no rock–fluid interaction or the mineral density and mass alteration cancel out) then,

$$\Delta V_b = \Delta V_p \quad (7)$$

If this assumption is valid then the porosity may be determined by combining equations (2, 4, 5 & 6)

$$\phi_{end,1} = \frac{V_p + \Delta V_b}{V_b + \Delta V_b} = \frac{\phi_0 - \varepsilon_{vol}}{1 - \varepsilon_{vol}} \quad (8)$$

Equation (8) is referred to as method 1 in the porosity calculations.

The second way of estimating the porosity after the test (method 2) relies on the difference between

the saturated and dry masses after the test in combination with equation (3),

$$\phi_{\mathrm{end},2} = \frac{(M_{\mathrm{sat,end}} - M_{\mathrm{dry,end}})}{\rho_{\mathrm{dw}} V_{\mathrm{b,end}}} \quad (9)$$

The third way of quantifying the porosity is by using pycnometry measurements. After the core was dismantled from the triaxial cell and the dry and saturated masses were obtained, it was cut into 7 slices. To provide more accurate solid volume measurements in the pycnometer the slices were grouped into 3 sets (s1 + s2, s3 + s4 + s5 and s6 + s7, see Fig. 4). Using the solid volume and mass we estimated the average mineral density of each set ($\rho_{\mathrm{s},i}$) from,

$$\rho_{\mathrm{s},i} = \frac{M_{\mathrm{dry},i}}{V_{\mathrm{s},i}} \quad (10)$$

where $i = 1, 2, 3$. The average solid mineral density of the whole core after flooding was calculated from the weighted average (by volume),

$$\rho_{\mathrm{s,end}} = \frac{V_{\mathrm{s},1}\rho_1 + V_{\mathrm{s},2}\rho_{\mathrm{s},2} + V_{\mathrm{s},3}\rho_{\mathrm{s},3}}{\sum_i^3 V_{\mathrm{s},i}} \quad (11)$$

With these data we could estimate the porosity by combining the average solid density ($\rho_{\mathrm{s,end}}$), the dry mass ($M_{\mathrm{dry,end}}$) and bulk volume ($V_{\mathrm{b,end}}$) after the experiment

$$\phi_{\mathrm{end},3} = \frac{V_{\mathrm{p}}}{V_{\mathrm{b}}} = 1 - \frac{V_{\mathrm{s}}}{V_{\mathrm{b}}} = 1 - \frac{M_{\mathrm{dry,end}}}{V_{\mathrm{b,end}}\rho_{\mathrm{s,end}}} \quad (12)$$

Equation (12) is referred to as method 3 for estimating the porosity after the test. By comparison we see that methods 2 and 3 take changes in mass and density into account, while method 1 only considers the volumetric strain changes.

Results

Porosity calculations before and after the experiment

The porosity of the tested chalk before the experiment based on the pore volume and the bulk volume (according to equation 3) is 43.45% and 43.43% for L1 and L2, respectively (Table 2). After flooding tests, $\varepsilon_{\mathrm{vol}}$ for L1 (9.4%) is larger than for L2 (5.1%) although both the total creep times and the effective stresses were higher for the L2 test than for compared with the L1 test (the L1 $MgCl_2$-flooded core was tested for 65 days at an effective stress of 9.5 MPa while the L2 NaCl-flooded core was tested for 90 days at 10.5 MPa). The effective stress during creep was set to be 2 MPa above the yield stress for both experiments (7.5 and 8.5 MPa for L1 and L2, respectively. See Fig. 2). The time evolution in the observed creep for the L1 test in Figure 3 displays an intriguing effect: at *c.* 35–40 days the axial creep rate increased. A similar acceleration in the creep rate induced by $MgCl_2$ flow was observed by Madland *et al.* (2011). This accelerated creep behaviour is not observed when the core is flooded by more inert brines such as NaCl. With time, the brine composition is the dominant factor, together with the effective stress, in determining the total observed volumetric deformation.

After the experiments, the dry mass changed for both cores. In the $MgCl_2$-flooded core (L1) 2.1 g was lost, which corresponds to 1.87% over 65 days. The NaCl-flooded core (L2) lost a mass of 0.54 g, corresponding to 0.43% (see Table 2) over 90 days. Hence, the $MgCl_2$ brine is more reactive towards the chalk than the NaCl brine. Given a specific density of approximate 2.70 g cm^{-3}, the mass losses for L1 and L2 correspond to solid volume losses of 1.09 and 0.20 cm^3, respectively. The weight difference between the DW-saturated cores and the dried cores was used to calculate the pore volume. For L1 the pore volume changed from 32.27 cm^3 before the test to 27.10 cm^3 after the test, while for L2 the pore volume changed from 36.07 cm^3 to 32.34 cm^3. At the same time the bulk volume changed from 74.26 cm^3 to 67.27 cm^3 for L1 and from 83.05 cm^3 to 78.77 cm^3 for L2. The average density of L1 increased from 2.68 g cm^{-3} to 2.70 g cm^{-3}, while there is no change in density for L2 after the experiment (Table 2). The resulting porosities that were calculated according to the three methods (in equation 8, 9 & 12) are shown in Table 2. For L1, method 1 (from the volumetric strain) results in a porosity reduction from 43.45% to 37.63%. However when using methods 2 and 3, which include the mass and density alterations in addition to the volume after the test, the porosity calculation revealed a smaller reduction than for method 1. The porosity changed from 43.45% to 40.29% and 39.28% for each method. The porosity estimates from method 1, 2 and 3 for L2 are 40.42%, 41.06% and 40.77%, respectively, from the original porosity of 43.43%. The L2 core shows a smaller variation in the porosity values from the three methods compared to the L1 core. By including the effect of chemical alteration in the porosity calculation, the difference in the final porosity between the $MgCl_2$- and NaCl-flooded cores is less significant, even though total volumetric strain is close to factor of two higher for the $MgCl_2$-flooded core (Table 2).

Effluent chemistry

The chemical analysis of the effluent during injection of $MgCl_2$ and NaCl confirms that chemical reactions occur inside the cores, as shown by the difference in both the density and the mass after flooding. Throughout the experiment the effluent from the $MgCl_2$-flooded core (L1) is depleted in Mg^{2+} ions (see Fig. 5a). The average Mg^{2+} ion concentration of the effluent is 0.202 mol l^{-1} in comparison with the 0.219 mol l^{-1} concentration of the injected brine, i.e. it is depleted by -0.017 mol l^{-1}. On the other hand, the average calculated Ca^{2+} concentration of the effluent water is 0.021 mol l^{-1}, corresponding to a net gain in the core material. The sum of the magnesium and calcium ion concentrations in the effluent (*c.* 0.222 mol l^{-1}) is, however, reasonably close to the injected $MgCl_2$ concentration (0.219 mol l^{-1}; Table 1), such that stoichiometry is almost preserved, indicating that a one-to-one ion exchange reaction occurs. Hence, the tested core experiences a significant magnesium gain and calcium loss. At the same time, the injected chloride reaches its original concentration (0.438 mol l^{-1}; Table 1) after only one test day (i.e. one PV see Fig. 5a). It should be noted that the number of test days includes the loading phase.

As can be seen in the lower plot in Figure 5b from the NaCl-flooded core (L2), the Na^+ and Cl^- ions reached their original concentrations (0.657 mol l^{-1}) after only one test day. Thereafter, the concentrations of Cl^- (0.653 mol l^{-1}) and Na^+ (0.654 mol l^{-1}) stayed constant during the whole experiment (see Fig. 5b). The calcium concentration of the effluent increased to a maximum value of 0.013 mol l^{-1} before decreasing to constant value around 0.001 mol l^{-1} after *c.* 7–8 days. These fluid flux and compositional data indicate that nearly 0.4 g of calcium carbonate was dissolved from the core, which agrees well with the loss in mass in Table 2.

FEG-SEM

The chalk from Liège is a relatively pure coccolithic mudstone; EDS analyses indicate more than 51 wt% CaO. Although the chalk contains only small quantities of non-calcite minerals, SEM micrographs document the widespread occurrence of submicrometre-sized quartz as well as clay minerals and other phyllosilicates (see Fig. 6 for an SEM micrograph of untested Liège chalk). Qualitative EDS measurements show that the dominant silicate phase is SiO_2 (*c.* 4.5 wt%), while other oxides occur in very low amounts: 0.9 wt% Al_2O_3, 0.3 wt% MgO and 0.02 wt% Na_2O.

No alteration is observed using SEM-EDS in the L2 core with NaCl injection. Neither imaging nor qualitative EDS measurements indicate any compositional changes induced by the injection of the brine. In contrast, the core flooded with the $MgCl_2$ solution shows significant changes in the mineralogical composition (Fig. 7). After the injection of the $MgCl_2$ brine into Liège chalk, the amount of magnesium is strongly increased (Table 4), with MgO contents of up to 3.2 wt% after 65 days of flooding. SEM imaging shows that highest magnesium contents are encountered in aggregates of newly formed submicrometre-sized crystallites scattered in the chalk. These crystallites are most commonly

Fig. 6. SEM micrograph of Liège chalk before flooding. Scale bar, 2 μm.

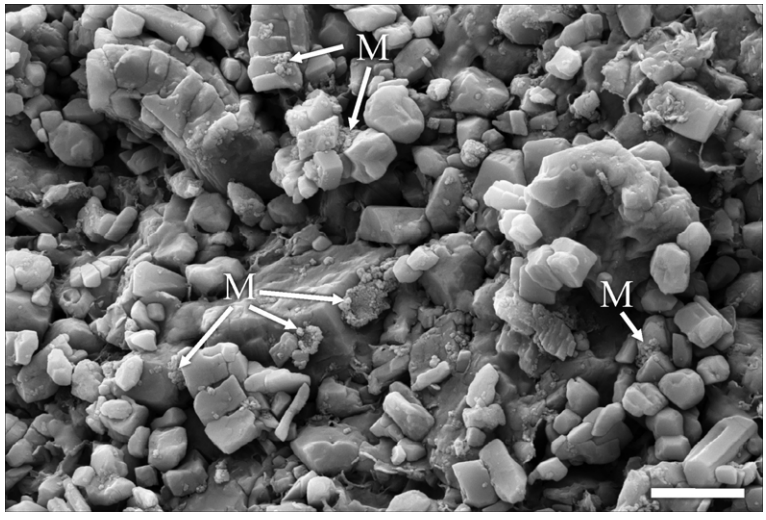

Fig. 7. SEM micrograph of Liège chalk after flooding with $MgCl_2$. Scale bar, 2 μm. M, Mg-rich carbonates or magnesite formed on top of pre-existing calcite grains.

observed close to the inlet and decrease in abundance along the core. Because of a relatively large sample interaction volume, the composition of grains smaller than *c.* 1 μm cannot unequivocally be determined using EDS as the signals from the new mineral phase and the primary calcite are mixed. However, the EDS measurements indicate that magnesium-rich carbonate minerals are being formed, in agreement with results from an experiment lasting 516 days with continuous flooding of an $MgCl_2$ solution (Zimmermann *et al.* 2015), and a 1072-day chemo-mechanical flow test using the same $MgCl_2$ solution (Nermoen *et al.* 2015), where a complete chemical re-working was documented.

XRD

The chalk from Liège appears to be homogeneous in XRD studies. Besides calcite, only very scarce quartz and traces of feldspar can be identified (see the 1L-d and 2L-d in Figs 8 & 9). The samples from the NaCl-flooded core (L2 in Fig. 9) contain slightly more quartz and feldspar compared to the L1 core (in Fig. 8). In the L1 experiment ($MgCl_2$ brine), the XRD analyses identified larger amount of Mg-bearing minerals in slice FL1-3 than slice FL1-1 (Fig. 8). Slice FL1-3 (Fig. 8) shows scarce magnesite and traces of a phase that could correspond to norsethite (peaks marked with an asterisk in Fig. 8), while traces of high-Mg calcite (Brown 1980) have been found in slice FL1-4. In L2 (NaCl-brine) no significant mineralogical changes are observed on the XRD patterns (Fig. 9).

Whole-rock geochemistry and isotope geochemistry

The chalk from Liège is also relatively homogeneous in terms of its geochemistry, reflecting the homogeneous mineralogy documented in Table 5. Table 4 shows the variation of four selected samples taken from the same block, which is compared with an average value of chalk from the same exposure ($n = 10$; unpublished data by Zimmermann). CaO concentrations are around 54.04 wt% and MgO abundances are as low as 0.27–0.29 wt%. SiO_2 varies only slightly along the core. Traces of clastic materials have been introduced to the chalk as observed from the sum of all rare earth elements (ΣREE), which increases faintly in between the samples (Table 4B). Although the samples have been taken from the same block, $\delta^{13}C_{SMOW}$ (where SMOW indicates Vienna Standard Mean Ocean Water) isotope values vary between 1.495‰ and 1.803‰ and $\delta^{18}O_{SMOW}$ between −2.049‰ and −1.607‰ (Table 4B), which therefore reflects the natural variation in stable isotopes for this rock material.

After flooding with NaCl (L2), the chalk does not show any significant geochemical changes (Table 4). $\delta^{13}C_{SMOW}$ values are similar to the unflooded samples of the chalk and only $\delta^{18}O_{SMOW}$ values are slightly more negative (Table 4). When the chalk was flooded with $MgCl_2$ significant changes in the MgO and CaO contents are observed. The amount of MgO increased from 0.28 wt% to 1.85 wt% (i.e. from 0.31 g to 2.05 g; highlighted in grey in Table 4), while the CaO concentration

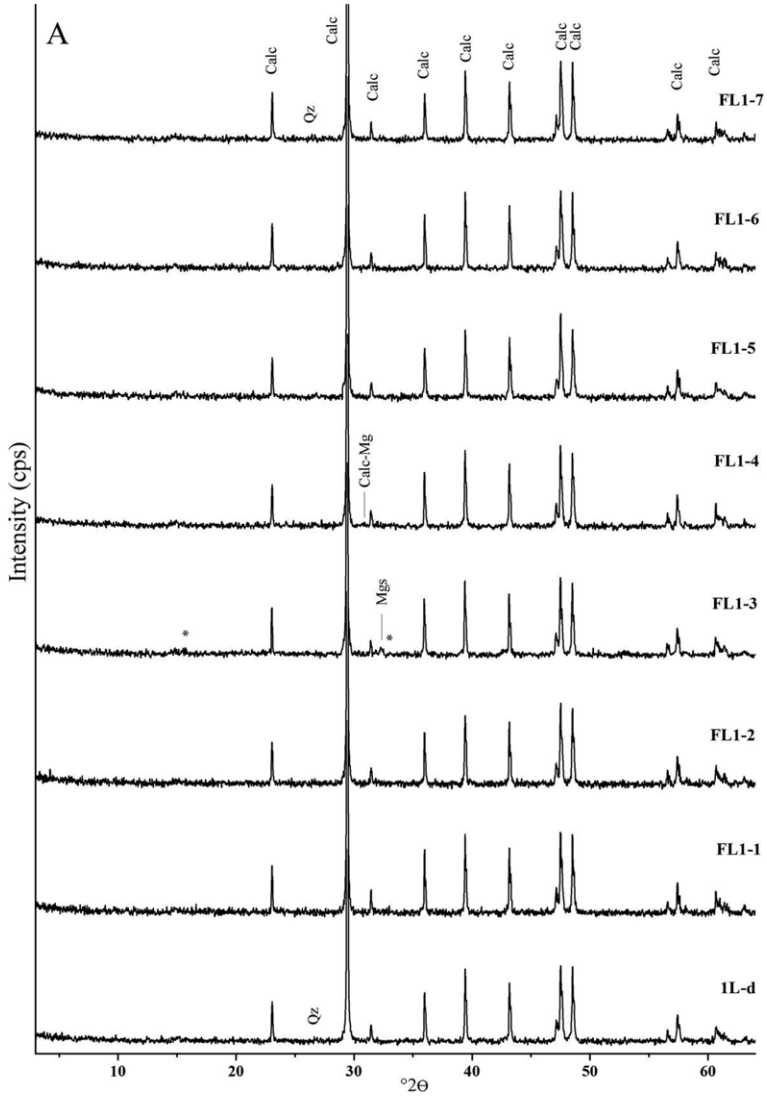

Fig. 8. XRD patterns of unflooded and $MgCl_2$-flooded Liège chalk (test L1). FL1-1 to FL1-7 are the seven slices that were acquired along the core axis (see Fig. 4) and 1L-d is the unflooded chalk. Calc, calcite; Mgs, magnesite; Calc-Mg, for Mg calcite; Feld, feldspars; Qz, quartz; the star symbols (*) mark peaks matching those of norsethite.

decreased from 54.04 wt% to 52.32 wt%, which corresponds to a net weight of 60.73 g before and 57.70 g after the experiment. However, the absolute weight per cent increase of MgO is almost exactly equal to the decrease in CaO at around 1.6 wt% (Table 4), indicating a correlation. Interestingly, it can also be observed that slice 3 reveals a higher MgO composition than slice 1. The reasons for the observed spatial dynamics along the core are complex and deserve further study. The alteration profile also is probably influenced by the interaction between the fluid flux and reaction kinetics. The only other element with significant changes in flooded L1 is Sr, which decreased after flooding.

Discussion

Our experiments indicate that geochemical reactions between the injected pore fluids and the rock mass may impact both the porosity and the

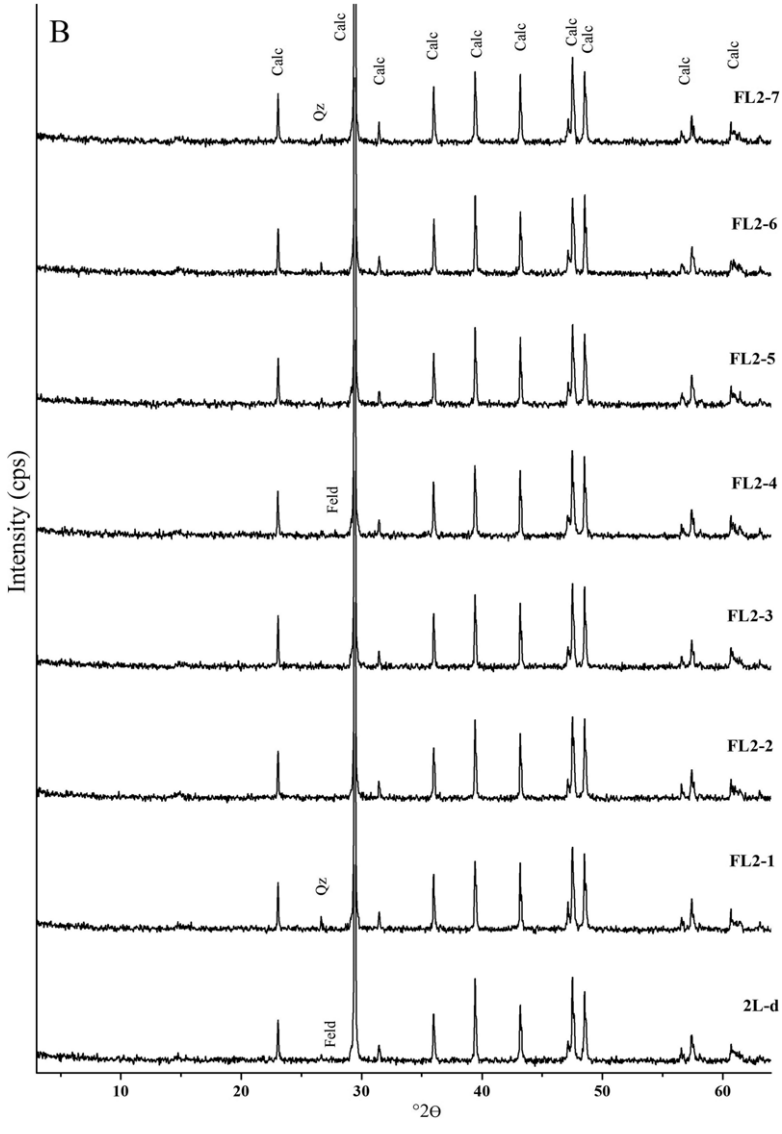

Fig. 9. XRD patterns of unflooded and NaCl flooded Liège chalk (test L2). FL2-1 to FL2-7 are the seven slices that were acquired along the axis of the core (see Fig. 4) and 2L-d is the untested Liège chalk. Calc, calcite; Feld, feldspars; Qz, quartz.

geomechanical behaviour during loading and creep. In particular, flooding of the chalk sample by $MgCl_2$ brines (L1) resulted in a reduction in the solid mass as well as an increase in the average solid density as calcite dissolved and Mg-bearing phases precipitated. A control experiment (L2) involving the flooding of a comparable sample by an NaCl brine, in contrast, showed much smaller geochemical alterations than the $MgCl_2$-flooded core. The L1 experiment (with geochemical alteration) shows greater volumetric strain compared with the control experiment, indicating that chemical reactions affect the overall volumetric creep.

Detailed SEM-EDS analyses revealed that minerals with a significant amount of MgO are abundant in the inlet of the core and slightly decrease through the sample (see the SEM images of unflooded chalk in Fig. 6 and flooded chalk in Fig. 7). This is confirmed by quantitative whole-rock geochemistry, which points to a 2 g increase in MgO

Table 5. *Comparison of the isotope geochemistry and geochemistry of the unflooded samples presented in this study (§) and the lower end, upper end and average values (#) for the Liège samples from Wang* et al. *(2013)*

	SiO_2 (%)	Al_2O_3 (%)	Fe_2O_3 (%)	MgO (%)	CaO (%)	Na_2O (%)	K_2O (%)	TiO_2 (%)	P_2O_5 (%)	MnO (%)	LOI (%)	Sum (%)	Ba (ppm)	Rb (ppm)	Sr (ppm)	Zr (ppm)	Y (ppm)	ΣREE (ppm)	Total carbon (%)	$\delta_{13}C_{SMOW}$ (‰)	$\delta_{18}O_{SMOW}$ (‰)	Temperature estimate (°C)
3L-A	2.01	0.35	0.13	0.27	54.14	0.05	0.08	0.02	0.12	0.02	42.7	99.86	36.0	3.4	945.6	6.9	8.1	26.3	12.19	1.550	−1.574	18.4
3L-B	2.00	0.35	0.19	0.26	53.86	0.05	0.08	0.02	0.13	0.02	42.9	99.85	41.0	3.7	961.8	7.7	8.5	24.3	12.02			
4L-A	1.84	0.32	0.12	0.27	54.20	0.04	0.07	0.02	0.14	0.02	42.8	99.87	32.0	3.0	887.8	7.5	8.5	23.0	12.15	1.578	−1.633	18.7
4L-B	1.83	0.32	0.14	0.27	54.34	0.05	0.07	0.02	0.14	0.02	42.7	99.86	35.0	3.0	915.5	9.2	8.7	25.0	12.05			
5L-A	1.87	0.33	0.12	0.26	54.59	0.04	0.07	0.02	0.10	0.02	42.4	99.86	35.0	3.1	959.9	6.5	7.7	22.9	12.15	1.502	−1.751	19.2
5L-B	1.83	0.32	0.13	0.26	54.39	0.04	0.08	0.02	0.10	0.02	42.6	99.84	38.0	3.1	958.6	6.5	7.7	23.3	12.05			
6L-A	1.99	0.32	0.16	0.25	54.13	0.04	0.07	0.02	0.08	0.02	42.7	99.84	38.0	3.2	973.0	8.2	6.9	22.7	11.97	1.511	−1.676	18.9
6L-B	2.03	0.32	0.14	0.25	54.34	0.04	0.06	0.02	0.09	0.02	42.5	99.85	39.0	2.8	968.5	7.5	7.0	24.0	12.17			
7L-A	2.03	0.36	0.13	0.26	54.19	0.04	0.08	0.02	0.08	0.02	42.6	99.85	37.0	3.9	932.6	8.0	7.9	22.2	12.25	1.618	−1.709	19.0
7L-B	2.06	0.37	0.14	0.26	54.04	0.04	0.08	0.02	0.09	0.02	42.7	99.85	35.0	3.7	952.3	7.0	8.0	24.6	12.13			
# (average)	1.95	0.34	0.14	0.26	54.22	0.04	0.07	0.02	0.11	0.02	42.66	99.85	36.6	3.3	945.6	7.5	7.9	23.8	12.11	1.552	−1.669	18.8
§ (average)	2.04	0.35	0.20	0.28	54.11	0.05	0.08	0.02	0.10	0.02	42.70	99.86	32.00	2.9	953.0	6.7	8.0	23.6	11.90	1.626	−1.793	19.4

$n = 10$	SiO_2 %	Al_2O_3 %	Fe_2O_3 %	MgO %	CaO %	Na_2O %	K_2O %	TiO_2 %	P_2O_5 %	MnO %	LOI %	SUM %
Lower	1.83	0.32	0.12	0.25	53.86	0.04	0.06	0.02	0.08	0.02	42.40	99.84
Upper	2.06	0.37	0.19	0.27	54.59	0.05	0.08	0.02	0.14	0.02	42.90	99.87
Average	1.95	0.34	0.14	0.26	54.22	0.04	0.07	0.02	0.11	0.02	42.66	99.85
§ (average)	2.04	0.35	0.20	0.28	54.11	0.05	0.08	0.02	0.10	0.02	42.70	99.86

$n = 10$	Ba (ppm)	Rb (ppm)	Sr (ppm)	Zr (ppm)	Y (ppm)	ΣREE PPM	Total C (%)	$\delta^{13}C_{SMOW}$ (‰)	$\delta^{18}O_{SMOW}$ (‰)	Temperature estimate (°C)
Lower	32.0	2.8	887.8	6.5	6.9	22.2	12.0			
Upper	41.0	3.9	973.0	9.2	8.7	26.3	12.3			
Average	36.6	3.3	945.6	7.5	7.9	23.8	12.1	1.566	−1.778	19.3
§ (average)	32.0	2.9	953.0	6.7	8.0	23.6	11.9	1.626	−1.793	19.4

$n = 10$ for geochemistry.

(*c.* 5–10× the original amount) in the flooded chalk (Table 4A). Values are not constant through the core and do not decrease from the inlet into the core, but vary from one slice to the next, surprisingly, the highest value for MgO is found in slice FL1-3. This trend is not yet understood, but may be related to differing microfacies or complex patterns of fluid flow through the chalk sample. However, the exact progress of the fluid–rock interplay can only be analysed when the involved chemical and mineralogical components are determined and quantified and coupled to the flow field within the sample. In addition, the alteration pattern is likely to reflect both the kinetics of the reaction and the fluid flux rates (Jones & Xiao 2005). The increase in MgO is probably associated with the formation of magnesite and Mg-bearing calcite. Other alteration products associated with the flooding process include norsethite, a Ba-rich carbonate associated with the dissolution of other carbonate phases (Gamsjäger *et al.* 1998). Zimmermann *et al.* (2013, 2015) propose that the lack of chemical equilibrium between the brine and the core triggers the dissolution of calcium carbonate and leads to the precipitation of Mg-bearing minerals. In long-term tests, new growth of magnesium carbonate could be verified with SEM-EDS studies, XRD analyses, nanoSIMS (nano secondary ion mass spectrometry) observations and oxygen isotopic data (Zimmermann *et al.* 2013). The solid volume could be affected by the chemical reaction between the rock and the fluid (Ruiz-Agudo *et al.* 2014; Nermoen *et al.* 2015). In the L1 experiment ($MgCl_2$ flooding test for 65 days), the bulk volume and solid volume decreased (Table 2) and the density increased (Table 3) because of calcium dissolution and the precipitation of new minerals. The solid volume is given by ratio of the solid mass and the average mineral density. Consequently, the geochemical alterations change the volume of the solids. Changes in both the bulk volume and the solid volume therefore need to be incorporated into porosity calculations when chemo-mechanical flow experiments are being interpreted.

When calculating the resulting porosity for the $MgCl_2$-flooded core (L1) with method 1, the volumetric strain only results in a porosity of 37.63%, indicating an absolute decrease of 5.82% (Table 2). When applying method 2 the calculated porosity is only 40.29%, i.e. an absolute reduction of less than 3.16%. By using the solid density measurement (pycnometry, method 3), the porosity reduces by about 4.17% (see Table 2). Methods 2 and 3 provide more accurate porosity values because they take into account the chemical alteration of the solid volume in addition to the volumetric strain, whereas method 1 only considers only the bulk volumetric strain. Therefore, coupling the volumetric strain directly to porosity is inadequate when chemical reactions occur. In the L1 experiment Mg–Ca exchange led to the formation of magnesite and high-Mg calcite and the dissolution of calcite.

In contrast, the results from the L2 experiment (the NaCl-flooded core), the effluent concentration changes are quite modest during the test, given that the sodium and chloride concentrations are similar to the injected ion concentrations (Fig. 5b). In addition, the SEM-EDS analyses do not reveal any new mineral growth and the whole-rock geochemistry shows no significant changes for the samples before and after flooding (Table 4A, B). In this experiment, the porosity calculations are rather similar for all three methods without the systematic differences that are seen in the L1 experiment. This lack of chemical alteration is consistent with geochemical, SEM and XRD data. However, the NaCl experiment (L2) may have dissolved some of the chalk (it lost *c.* 0.54 g over 90 days). It is therefore valid to use method 1 to estimate the porosity development as the reaction rate is slow for L2 when compared with the total volume of the injected fluid and the duration of the experiment.

There are always uncertainties associated with experimental work. Here, we discuss how experimental error may affect our conclusions regarding the porosity estimate. The porosity is estimated using three methods. For method 2 the porosity estimates originate from the saturated and dry weight difference according to equation (9). Here, the errors are attributed to the weight measurements and bulk volume estimates (from the truncated wedge in equation 4). Repeated bulk volume estimates display a natural variability on the order of 0.1–0.2 ml. During the DW saturation procedure only partial saturation could occur, which would yield an underestimate of the saturated weight and thus an underestimate of the porosity using this technique. However, the pycnometry tests (see Table 3) can be used to measure the solid density, which can be used to estimate the initial solid volume. If the bulk volume is known, the pore volume can be estimated from equation (1). The pore volume measurement from the pycnometry measurement and from the DW saturation and drying indicates an initial saturation of more than 99.5% for both tests. The dry weight of the plugs was measured after the plug had been placed in a heating cabinet until the weight is stable (at least 24 h). The repeatability in the porosity estimate from method 2 originates from errors in the bulk volume as well as in the saturated and dry weights and adds up to less than 1%. In order to gain certainty in the estimates the pycnometry measurements using method 3 in equation (12) are applied. Method 3 is partially independent of method 2 and may therefore provide a complementary estimate to method 1. Here, the largest error source is attributed to the solid volume

estimate from the helium gas pycnometry. On the basis of repeatability tests the solid density is estimated within ± 0.02 g cm^{-3}. Errors of this magnitude in the solid density measurements yield porosity errors on the order of $<0.5\%$. In method 1, the porosity is estimated from the volumetric strain measurements from the bulk volume measurements before and after the test (see equation 5). This estimate is mathematically correct under the assumption that the total solid volume is conserved during compaction. The source of error is found in the bulk volume measurements after the test. Before the test the diameters along the plug vary by less than 0.01 mm. However, after hydrostatic compactionthis is not the case and the varying diameters are accounted for by calculating the volumes of the truncated wedge.

The resulting changes in the produced effluent concentrations, and the post-experimental analysis of the tested chalk sample, demonstrate that mineral reactions occur that change the volume. These changes are linked to the dissolution of Ca-bearing minerals, and the precipitation of Mg-bearing minerals. These mineralogical changes, exemplified by dissolution of e.g. calcium carbonate (density 2.69 g cm^{-3}) and the precipitation of magnesite (density of 3.00 g cm^{-3}), lead to measurable volume changes. It should be noted that the solid volume changes may be explained by both differences in the solid mass and the solid density in equation (13). In the L1 test (flooded with $MgCl_2$) a mass loss of 2.1 g and a density increase of 0.03 g cm^{-3} were both observed in slice 1 and the change in the solid volume is 1.09 cm^3, while for L2 the solid volume is changed by only 0.20 cm^3 (see Table 2).

Conclusions

Chemo-mechanical experiments on the Upper Cretaceous onshore chalk from Liège with 0.657 M NaCl and 0.219 M $MgCl_2$ brines at Ekofisk temperatures have revealed that both mechanical compaction and dissolution/precipitation reactions play a role in the porosity development. By contrast, mechanical compaction alone is the primary cause of porosity loss in a companion experiment involving an NaCl brine. A chalk sample that has been flooded with $MgCl_2$ shows significant changes in the rock chemistry. Total MgO in the core increases from 0.3 g to 2.05 g and a similar decrease is observed for CaO. This observation was confirmed by whole-rock geochemistry, effluent chemistry and SEM-EDS observations. The latter provides evidence for the precipitation of magnesium calcite or even magnesite. XRD analyses show scarce magnesite and minute amounts of high-Mg calcite. The geochemical alteration associated with $MgCl_2$ flooding changed the geomechanical properties of the chalk by accelerating the strain rate.

An additional effect of the geochemical alteration is that the strain alone is not a sufficient basis for accurately determining the pore volume change. Porosity estimations for geochemically altered reservoirs must account for the effects of the reactions on the solid mass, the volume and the density (Nermoen *et al.* 2015). These geochemical effects result in more complex reservoir behaviour compared with mechanical compaction alone for non-reactive rock–fluid combinations. Such effects may markedly influence the outcome of EOR/IOR (improved oil recovery) operations in fields where injection fluids react with the reservoir rock. Precise porosity estimates are of crucial importance for accurate resource potential estimates and to predict the flow properties of reservoirs that are undergoing chemo-mechanical compaction processes.

The authors thank the Faculty of Science and Technology for the PhD grant for W. Wang. The authors thank COREC for financial support for this research study and all authors acknowledge the Research Council of Norway and the industry partners, ConocoPhillips Skandinavia AS, BP Norge AS, Det Norske Oljeselskap AS, Eni Norge AS, Maersk Oil Norway AS, DONG Energy A/S, Denmark, Statoil Petroleum AS, ENGIE E&P NORGE AS, Lundin Norway AS, Halliburton AS, Schlumberger Norge AS and Wintershall Norge AS of The National IOR Centre of Norway for support. The research presented is integral part of the PhD thesis of W. Wang at UiS. We also thank two anonymous reviewers and Peter Armitage as well as Ron Lander for their thoughtful comments, which improved the original manuscript. We also appreciate the handling by the editors.

References

Anderson, T.F. & Arthur, M.A. 1983. Stable isotopes of oxygen and carbon and their application to sedimentologic and environmental problems. *In*: Arthur, M.A., Anderson, T.F., Kaplan, I.R., Veizer, J. & Land, L.S. (eds) *Stable Isotopes in Sedimentary Geology*. SEPM Short Course Notes, **10**, 1–151.

Brown, G. 1980. Associated minerals. Chapter 6. *In*: Brindley, G.W. & Brown, G. (eds) *Crystal Structures of Clay Minerals and Their X-ray Identification*. Mineralogical Society Monographs, **5**, 361–410.

Felder, W.M. 1975. Lithostratigrafie van het Boven-Krijt en het Dano-Montien in Zuid-Limburg en het aangrenzende gebied. ('Lithostratigraphy of the Upper Cretaceous and the Dano-Montien in southern Limburg and the neighboring region.') *In*: Zagwijn, W.H. & Van Staalduinen, C.J. (eds) *Toelichting bij de geologische overzichtskaarten van Nederland*. Rijks Geologische Dienst, Haarlem, 63–72.

FJÆR, E., HOLT, R.M., HORSRUD, P., RAAEN, A.M. & RISNES, R. 2008. *Petroleum Related Rock Mechanics*. 2nd edn. Elsevier, Amsterdam.

GAMSJÄGER, H., KÖNIGSBERGER, E. & PREIS, W. 1998. Solubilities of metal carbonates. *Pure & Applied Chemistry*, **70**, 1913–1920.

HELLMANN, R., RENDERS, P.J.N., GRATIER, J.P. & GUIGUET, R. 2002. Experimental pressure solution compaction of chalk in aqueous solutions. Part 1. Deformation behavior and chemistry. *In*: HELLMANN, R. & WOOD, S.A. (eds) *Water Rock Interactions, Ore Deposits, and Environmental Geochemistry: A tribute to David A. Crerar*. The Geochemical Society, Special Publications, **7**, 129–152.

HIORTH, A., CATHLES, L.A., KOLNES, J., VIKANE, O., LOHNE, A., KORSNES, R.I. & MADLAND, M.V. 2008. A chemical model for the seawater-CO_2-carbonate system – aqueous and surface chemistry. Paper presented at the International Symposium of the Society of Core Analysts, Abu Dhabi, United Arab Emirates, 1–12.

HJULER, M.L. & FABRICIUS, I.L. 2009. Engineering properties of chalk related to diagenetic variations of Upper Cretaceous onshore and offshore chalk in the North Sea area. *Journal of Petroleum Science and Engineering*, **68**, 151–170.

JONES, G.D. & XIAO, Y.T. 2005. Dolomitization, anhydrite cementation, and porosity evolution in a reflux system: Insights from reaction transport models. *AAPG Bulletin*, **89**, 577–601.

KORSNES, R.I. 2007. *Chemical induced water weakening of chalk by fluid-rock interaction, A mechanistic study*. PhD thesis, University of Stavanger.

KORSNES, R.I., STRAND, S., HOFF, Ø., PEDERSEN, T., MADLAND, M.V. & AUSTAD, T. 2006*a*. Does the chemical interaction between seawater and chalk affect the mechanical properties of chalk?. *In*: COTTHEIUM, A.V., CHARLIER, R., THIMUS, J.F. & TSHIBANGU, J.P. (eds) *Eurock 2006. Multiphysics Coupling and Long Term Behaviour in Rock Mechanics*. The International Symposium of the International Society for Rock Mechanics, 9–12 May 2016, Liège, Belgium, 427–434.

KORSNES, R.I., MADLAND, M.V. & AUSTAD, T. 2006*b*. Impact of brine composition on the mechanical strength of chalk at high temperature. *In*: COTTHEIUM, A.V., CHARLIER, R., THIMUS, J.F. & TSHIBANGU, J.P. (eds) *Eurock 2006. Multiphysics Coupling and Long Term Behaviour in Rock Mechanics*. The International Symposium of the International Society for Rock Mechanics, 9–12 May 2016, Liège, Belgium, 133–140.

KORSNES, R.I., MADLAND, M.V., AUSTAD, T., HAVER, S. & RØSLAND, G. 2008. The effects of temperature on the water weakening of chalk by seawater. *Journal of Petroleum Science & Engineering*, **60**, 183–193.

MADLAND, M.V. 2005. *Water weakening of chalk: A mechanistic study*. PhD thesis, University of Stavanger.

MADLAND, M.V., MIDTGARDEN, K., MANAFOV, R., KORSNES, R.I., KRISTIANSEN, T.G. & HIORTH, A. 2008. The effect of temperature and brine composition on the mechanical strength of Kansas chalk. Paper presented at the International Symposium of the Society of Core Analysts, Abu Dhabi, United Arab Emirates, 29 October–2 November 2008, 1–6.

MADLAND, M.V., HOIRTH, A. *ET AL*. 2011. Chemical alterations induced by rock–fluid interactions when injecting brines in high porosity chalks. *Transport in Porous Media*, **87**, 679–702.

MADLAND, M.V., ZIMMERMANN, U. *ET AL*. 2013. Neoformed dolomite in flooded chalk for EOR processes. Paper presented at the 75th EAGE Conference & Exhibition incorporating SPE EUROPEC, 10–13 June 2013, London, UK.

MOLENAAR, N. & ZIJLSTRA, J.J.P. 1997. Differential early diagenetic low-Mg calcite cementation and rhythmic hardground development in Campanian-Maastrichtian chalk. *Sedimentary Geology*, **109**, 261–281.

NERMOEN, A., KORSNES, R.I., HIORTH, A. & MADLAND, M.V. 2015. Porosity and permeability development in compacting chalks during flooding of nonequilibrium brines: insights from long-term experiment. *Journal of Geophysical Research*, **120**, 2935–2960.

NEWMAN, G. 1983. The effect of water chemistry on the laboratory compression and permeability characteristics of some north sea chalks. *Journal of Petroleum Technology*, **35**, 976–980.

RUIZ-AGUDO, E., PUTNIS, C.V. & PUTNIS, A. 2014. Coupled dissolution and precipitation at mineral-fluid interfaces. *Chemical Geology*, **383**, 132–146.

SLIMANI, H. 2001. New species of dinoflagellate cysts from the Campanian–Danian chalks at Hallembaye and Turnhout (Belgium) and at Beutenaken (the Netherlands). *Journal of Micropalaeontology*, **20**, 1–11.

STRAND, S., HJULER, M.L., TORSVIK, R., PEDERSE, J.I., MADLAND, M.V. & AUSTAD, T. 2007. Wettability of chalk impact of silica, clay content and mechanical properties. *Petroleum Geoscience*, **13**, 69–80.

WANG, W., ZIMMERMANN, U., MADLAND, M.V., BERTOLINO, S.R.A., LIE, B.V. & MOROSOVA, V. 2013. The search of on-shore equivalents for reservoir chalk in the North Sea: Rare Earth Elements, $\delta^{13}C$ and $\delta^{18}O$ isotopes as indicators? Paper presented at Norsk Geologisk Forening Vinterkonferansen, Oslo, 8–10 January 2013, 112–113.

WIBORG, R. & JEWHURST, J. 1986. Ekofisk subsidence detailed and solutions accessed. *Oil and Gas Journal*, **2**, 47–51.

WRIGHT, E.K. 1987. Stratification and paleocirculation of the Late Cretaceous Western Interior Seaway of North America. *Geological Society of America Bulletin*, **99**, 480–490.

ZIMMERMANN, U., MADLAND, M.V., BERTOLINO, S.A.R., HILDEBRAND-HABEL, T., HIORTH, A. & KORSNES, R.I. 2013. Tracing fluid flow in flooded chalk under long term test conditions. Paper presented at the 75th EAGE Conference & Exhibition incorporating SPE EUROPEC, 10–13 June 2013, London, UK.

ZIMMERMANN, U., MADLAND, M.V. *ET AL*. 2015. Evaluation of the compositional changes during flooding of reactive fluids using SEM, Nano-SIMS, XRD and whole-rock geochemistry. *AAPG Bulletin*, **99**, 791–805.